Supporting Information

Self-assembly of ultra-thin lanthanide oxide nanowires via surfactant-mediated imperfect oriented attachment of nanoparticles

Fraser J. Douglas,[a] Carlos Renero-Lecuna,[b] Robert D. Peacock,[a] Rafael Valiente,[b] Donald A. MacLaren[c]* and Mark Murrie[a]*

[a] *WestCHEM, School of Chemistry, University of Glasgow, Glasgow G12 8QQ (UK), Fax: +44 141 330 4888, Tel: +44 141 330 4486, E-mail: Mark.Murrie@glasgow.ac.uk*
[b] *MALTA-Consolider Team, Dpt. Física Aplicada, Facultad de Ciencias, Universidad de Cantabria, 39005 Santander, Spain.*
[c] *SUPA, School of Physics and Astronomy, The University of Glasgow, Glasgow G12 8QQ (UK), Fax: +44 141 330 5886, Tel: +44 141 330 4464, E-mail: dmaclaren@physics.org*

Experimental Details

Transmission electron microscopy (TEM) and electron diffraction was performed on a FEI Tecnai T20 instrument equipped with a LaB_6 filament and operated at 200 keV.

High resolution TEM (HRTEM), Electron Energy Loss Spectroscopy (EELS) and Energy Dispersive X-ray (EDX) measurements were recorded on a FEI Tecnai TF20 instrument operated at 200 keV and fitted with a field emission gun, Gatan Enfina electron spectrometer and EDAX EDX detector.

Powder X-ray diffraction data were collected on a PANalytical X'Pert instrument. Samples were prepared by evaporating a nanowire dispersion onto a silicon support. IR spectra were obtained using a Shimadzu 8400s FT-IR. Thermogravimetric analysis was performed on a TA Instruments Q500 Thermogravimetric Analyzer under a nitrogen atmosphere. Room temperature photoluminesence measurements were recorded on an Edinburgh Instrument FLS920 spectrofluorometer and the spectra were corrected for the response of the detection system.

Materials and Methods

Lanthanide(III) chloride hydrate (99%), oleic acid 90%, oleyl amine 70%, sodium oleate (≥82%) and dioctyl ether (99%) were purchased from Sigma-Aldrich. Ethanol (analytical grade) and hexane (H.P.L.C. grade) were purchased from VWR International. All chemicals were used as received without further purification.

Synthesis of the oleate precursor
The synthesis of the oleate precursors was adapted from a previous method.[1] Using gadolinium oleate as an example, gadolinium chloride hexahydrate (6 mmol) was mixed with sodium oleate (18 mmol) in a mixture of hexane (21 mL), ethanol (12 mL) and water (9 mL). This mixture was refluxed at 70 °C for 4 hours then allowed to stir for a further 16 hours at room temperature. The upper organic layer containing the gadolinium oleate was removed, washed twice with deionised water and the hexane was removed under vacuum to yield gadolinium oleate as a waxy solid. An identical method was used to synthesise the other lanthanide oleates simply by using 6 mmol of the appropriate lanthanide chloride precursor.

Synthesis of the lanthanide oxide nanowires and ribbons
To make the nanowires, the lanthanide oleate precursor (0.5 mmol) was mixed in air with oleylamine (4 mL), oleic acid (3 mL) and dioctyl ether (2 mL) before being transferred to a 12 mL Teflon lined steel autoclave. The autoclave was then heated at 10 °C min^{-1} to 200 °C and maintained at this temperature for 24 hours. After allowing the autoclave to cool naturally, ethanol was added to the mixture to precipitate the particles, which were collected by centrifugation at 4,000 rpm for 10 minutes. To clean the particles, the residue collected after centrifugation was dispersed in 5 mL of hexane and re-precipitated with ethanol and centrifuged. This procedure was repeated at least 5 times to ensure the sample was clean enough for HRTEM experiments.

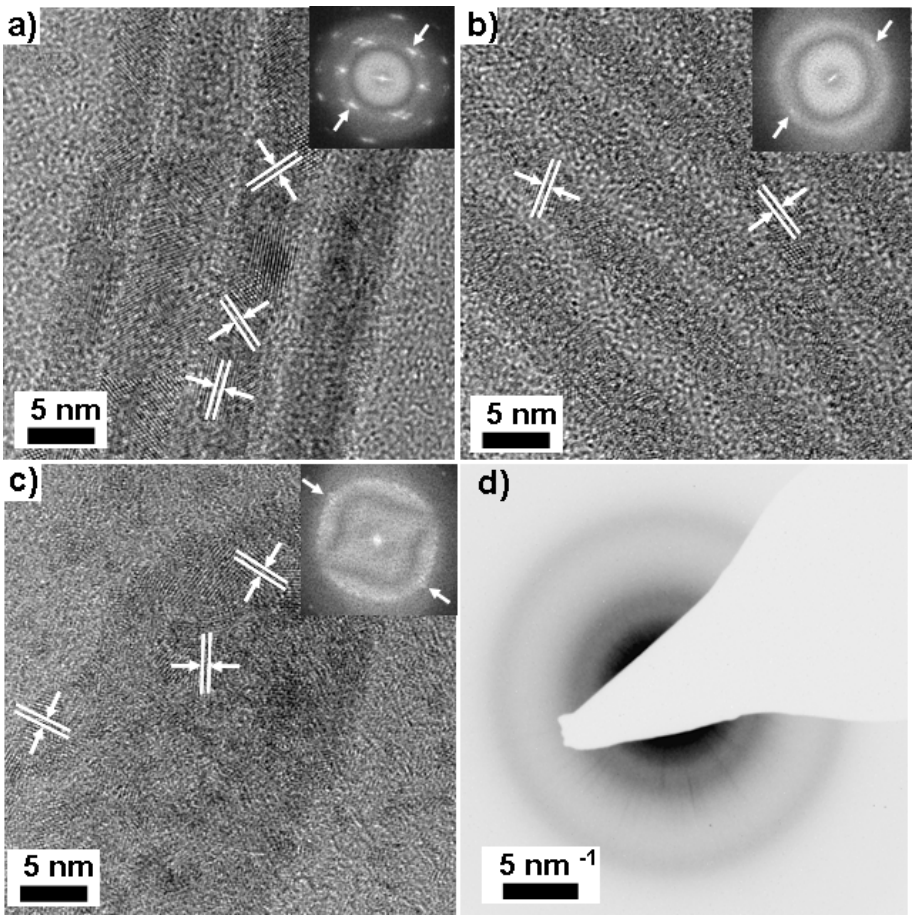

Figure S1. Additional HRTEM images for (a) CeO_2 nanowires, (b) Nd_2O_3 nanowires and (c) Dy_2O_3 nanoribbons supported by a 'holey carbon' film. The weak contrast between the Ln oxide materials and underlying carbon support film arises from the thinness of the oxides. Inset are the corresponding fast Fourier transforms (FFTs). The images highlight the material polycrystallinity. Interplanar distances for each of the crystalline regions examined were determined to be (a) 0.28 nm, (b) 0.27 nm and (c) 0.26 nm, consistent with cubic CeO_2 (200) and cubic Ln_2O_3 (400) reflections. Lattice constants were determined from (200) or (400) FFT spot distances (indicated with arrows) as (a) 0.528 ± 0.015 nm, (b) 1.094 ± 0.006 nm and (c) 1.056 ± 0.030 nm, which are in agreement with the reference cards mentioned in the main text.

The small size of the crystallites that comprise the wires for the mid- and late-series lanthanide oxides result in very weak scattering and diffuse electron diffraction rings, such as those for (d) Dy_2O_3.

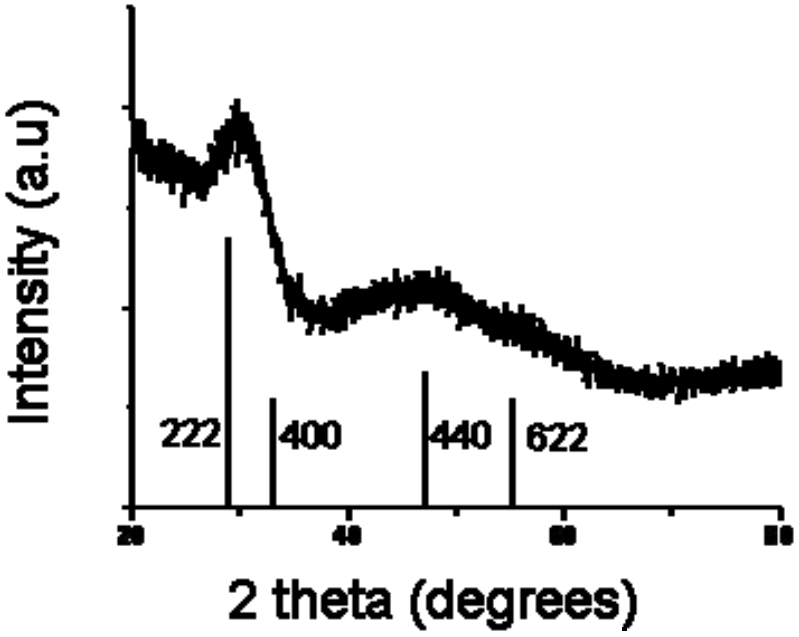

Figure S2. Illustrative powder X-ray diffraction (XRD) pattern of the as-obtained Gd_2O_3 nanowires, indexed to cubic *Ia-3* Gd_2O_3 (PDF card number 43-1014).

The average size of crystallites within the Gd_2O_3 sample was calculated using the Debye-Scherrer equation, which gave an average crystallite size of 2.86 nm. This value is in good agreement with the ~3 nm size determined by TEM.

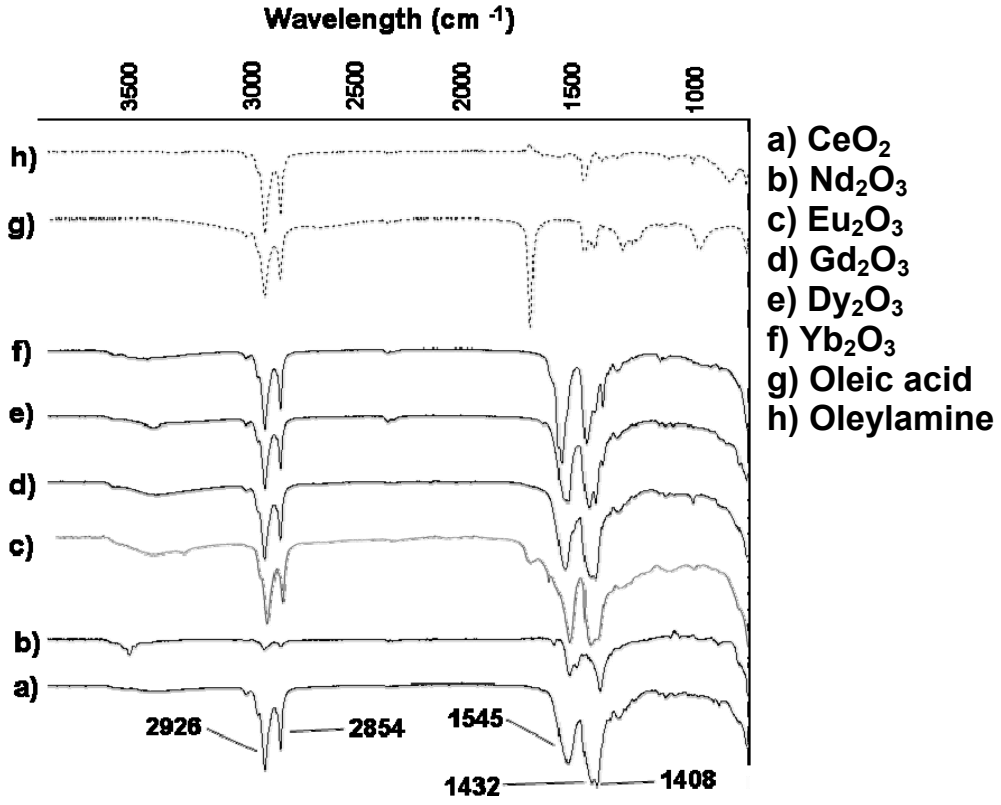

Figure S3. IR spectra of the as-obtained lanthanide oxide nanowire powders (a-f), oleic acid (g) and oleylamine (h). The powders are (a) CeO_2 (b) Nd_2O_3 (c) Eu_2O_3 (d) Gd_2O_3 (e) Dy_2O_3 and (f) Yb_2O_3.

The peaks at 2926 cm^{-1} and 2854 cm^{-1} are assignable to the antisymmetric and symmetric methylene stretches ($\nu_{as}(CH_2)$ and $\nu_s(CH_2)$) of oleic acid (g) and oleylamine (h). The antisymmetric methyl stretch, $\nu_{as}(CH_3)$, is observable as a shoulder on the 2926 cm^{-1} peak. These peaks show little difference to their counterparts measured from pure oleylamine and oleic acid. It has been previously reported that the IR spectra of OAm-coated particles is very similar to the IR spectrum of pure OAm, so it is anticipated that there is OAm on the particle surface.[2] The ν(C=O) stretch for pure oleic acid (g), appears at 1710 cm^{-1}. This peak is absent in the infrared spectrum of the LnOx nanowires (a-f), and is replaced with two characteristic bands at 1545 cm^{-1} and 1432 cm^{-1}, which are assignable to the antisymmetric ($\nu_{as}(COO^-)$), and symmetric, ($\nu_s(COO^-)$) stretches, respectively. The strength of these (COO^-) peaks suggests that OA is the predominant surfactant on the particle surface. The difference in wavenumber of these two (COO^-) stretches can be used to determine to mode of co-ordination of the carboxylate group of oleic acid to the lanthanide oxide nanowire surface. For a monodentate ligand a separation of >200 cm^{-1} is expected, <110 cm^{-1} for a bidentate and 140-200 cm^{-1} for a bridging ligand.[3] For our system the separation is 113 cm^{-1}, which suggests oleic acid on the particle surface is acting as a bidentate ligand, which is in agreement with literature observations.[4] The IR spectra of the as-obtained nanowires show no evidence for the presence of the OA/OAm condensation product [N-(*cis*-9-octadecenyl)-oleamide] on the particle surface, in agreement with other OA/OAm mixed solvent systems.[5]

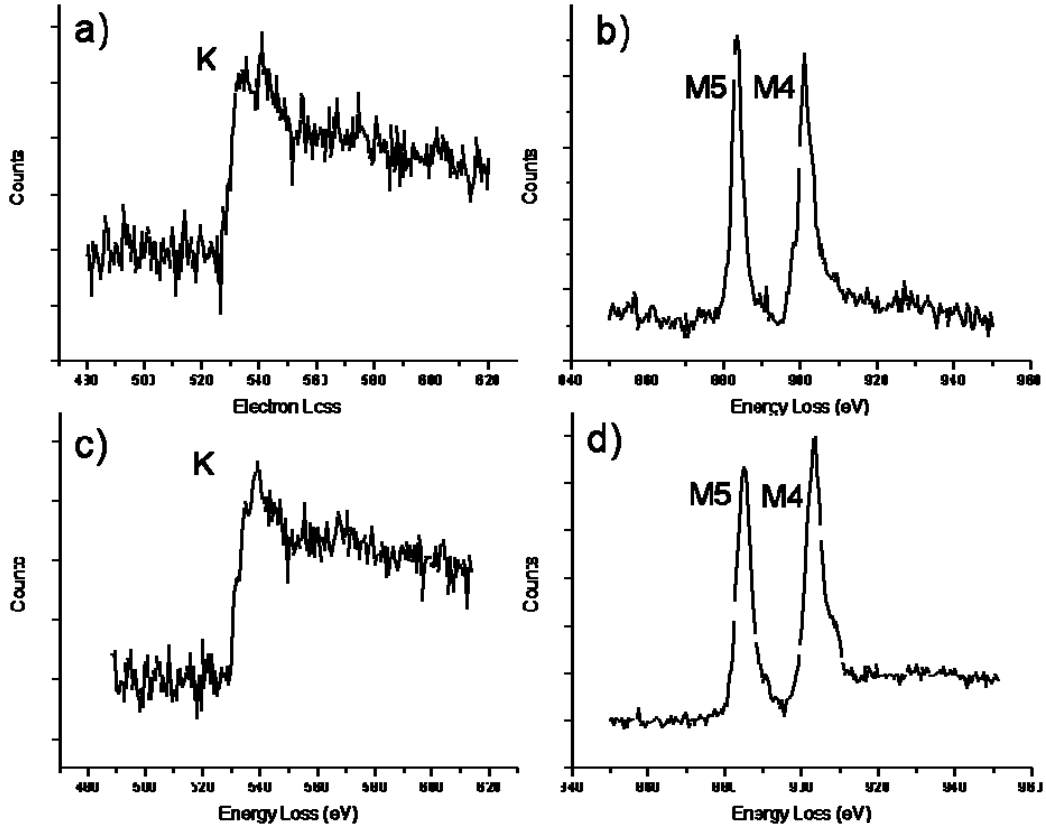

Figure S4 EELS spectra of the oxygen K and Ce M5, M4 edges of nanowires (a,b) immediately after synthesis and (c,d) following oxidation to CeO_2. The Ce M4/M5 edge ratio noticeably increases from (a) to (b), which is consistent with increasing oxidation state from Ce^{3+} to Ce^{4+}.[6] The elemental compositions were calculated as Ce 40.8 %, O 59.2 % and Ce 36.7 %, O 63.3 % before and after oxidation, respectively. Elemental compositions are determined using the Gatan Digital Micrograph software package, using Hartree-Slater electron scattering cross-sections and following removal of a fitted power-law background.

The variation of cerium oxidation state in CeO_2 nanomaterials has been studied before, and it has been shown that small (<15 nm) particles can be described as CeO_{2-x}, with x increasing to 0.5 towards the particle edge.[7] The decrease in oxygen levels at CeO_2 particle edges is attributed to the migration of oxygen vacancies in the CeO_2 unit cell towards the particle surface.[8] This means that small particles can have a stoichometry approaching Ce_2O_3, whilst retaining the cubic CeO_2 structure (note that cubic Ce_2O_3 does not occur in the bulk). Our EELS and SAED data would appear to confirm this. Upon exposure to air (such as during the washing cycle), any Ce^{3+} that is present is oxidized to Ce^{4+}, as was confirmed through EELS.

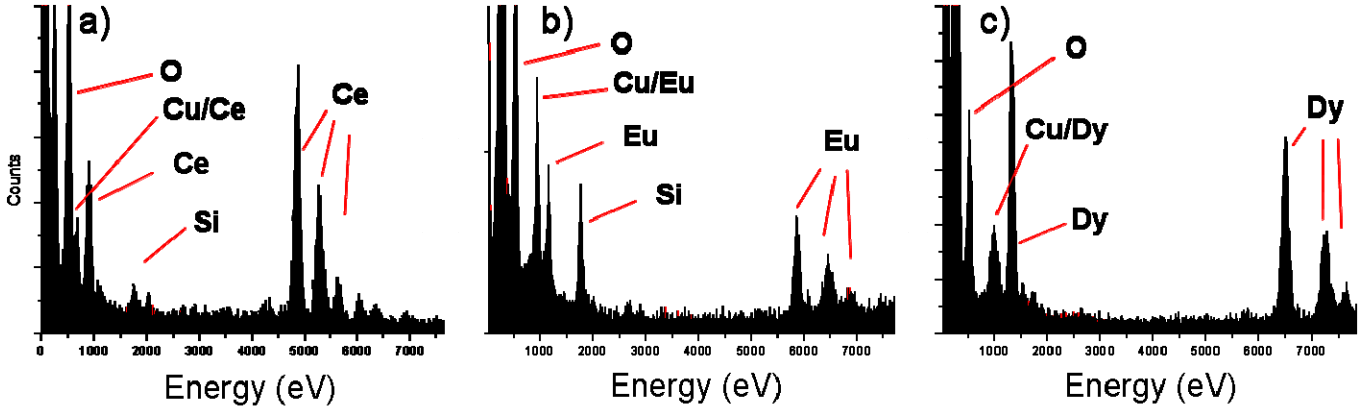

Figure S5 EDX spectra of (a) CeO_2, (b) Eu_2O_3 (c) Dy_2O_3 nanowires. The Cu and Si peaks are from the TEM grids used whilst a peak at very low energy corresponds to carbon from the 'holey carbon' support grid.

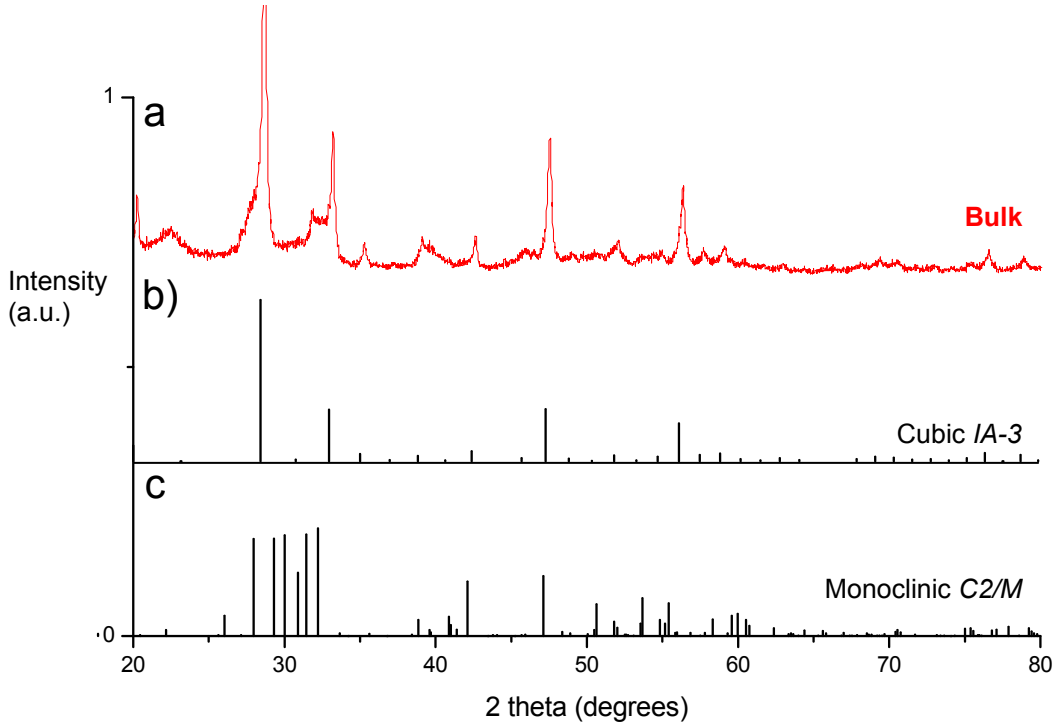

Figure S6 Powder XRD spectra of bulk Eu_2O_3 powder used in the PL measurements (Fig. 5 in the main text). Comparison with reference patterns for cubic (pdf card number 01-072-7065) and monoclinic (01-071-0589) confirms the bulk powder to be cubic (*Ia-3*) Eu_2O_3.

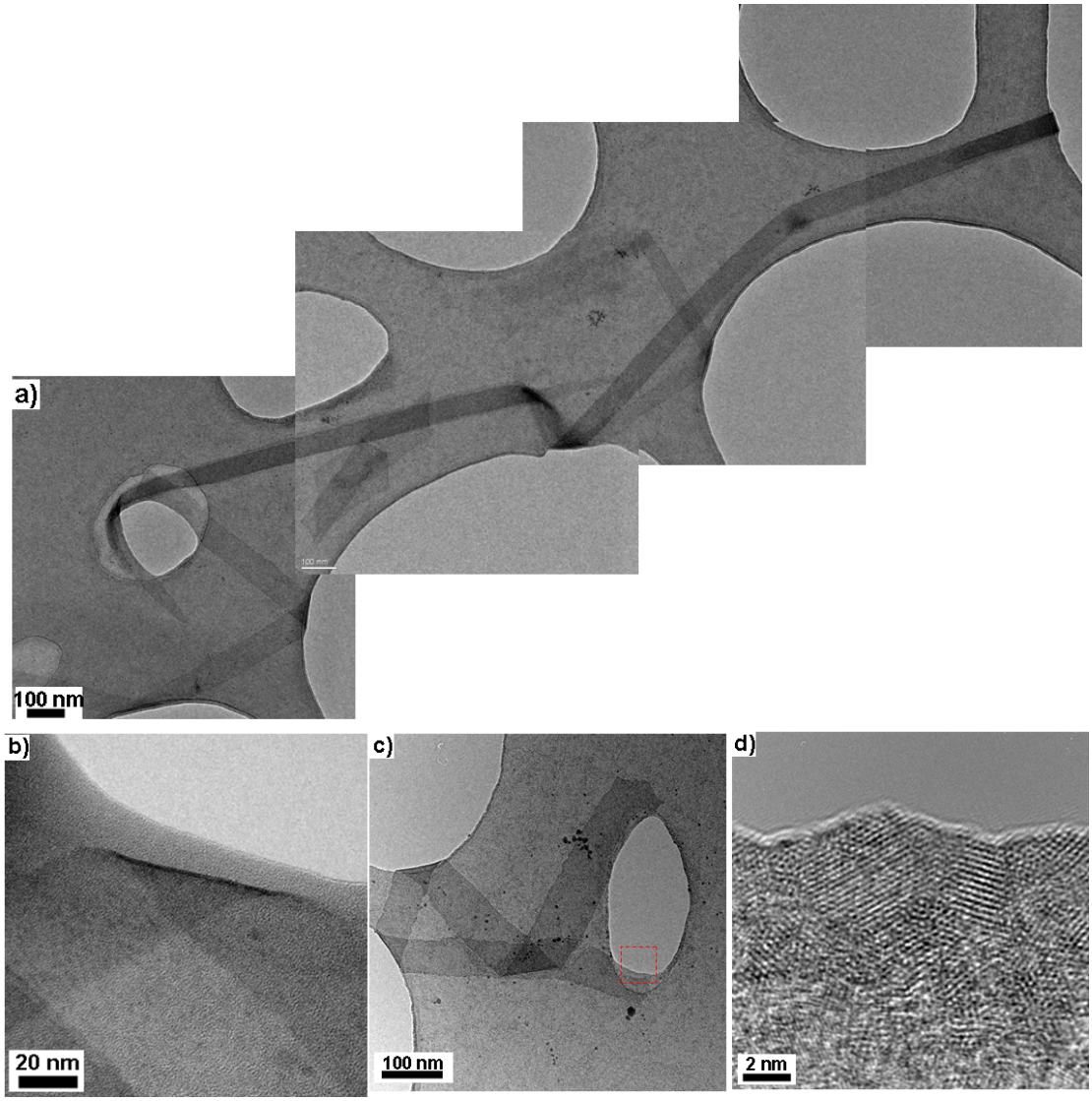

Figure S7 Additional TEM images of the Dy_2O_3 nanoribbon species. (a) The length of this particular ribbon is over 3 microns (~3150 nm). (b) HRTEM image showing a fold in the thin nanoribbon, illustrating its flexibility and mechanical stability under deformation. (c) TEM image of a shorter nanoribbon, also displaying a high degree of flexibility. The red box shows a fragment of nanoribbon that overhangs a hole in the underlying holey carbon film, corresponding to the area of HRTEM image, (d), which clearly shows the random orientation of crystallinity within a nanoribbon. The interplanar distance was determined to be 0.26 nm, consistent with cubic Dy_2O_3 (400) reflections.

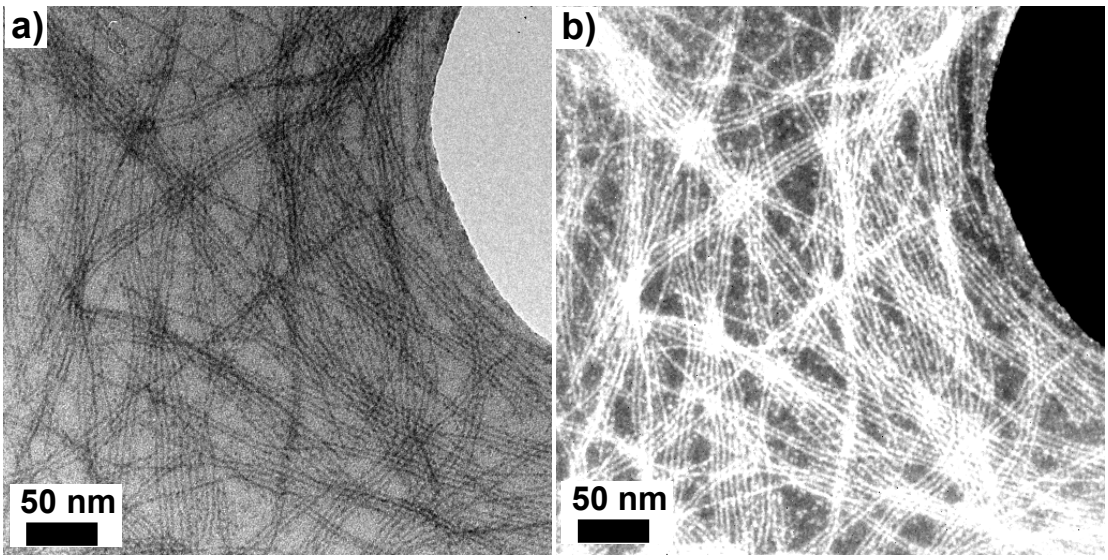

Figure S8. Bright field (a) and corresponding dark-field (b) images of Eu_2O_3 nanowires obtained from a 24 hour reaction. The images clearly show small ~3 nm particles (as a minority species) alongside the wires.

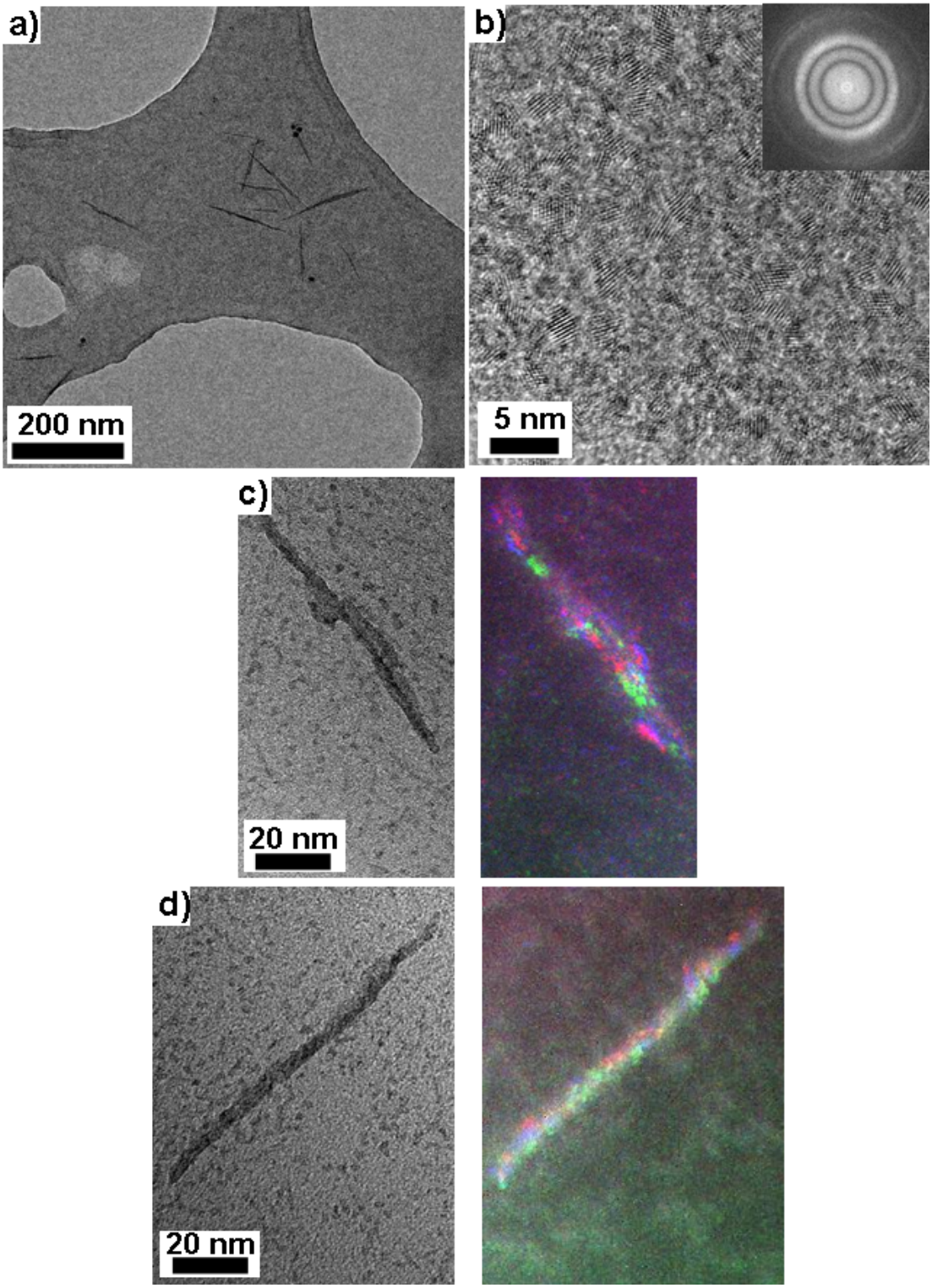

Figure S9. TEM images from a 4 hour reaction showing (a) short CeO_2 wires and (b) an abundance of small ~3 nm CeO_2 particles. Inset is the corresponding FFT. Further bright field / dark field pairs (c,d) highlight the variation in crystal structure along the length of a short wire.

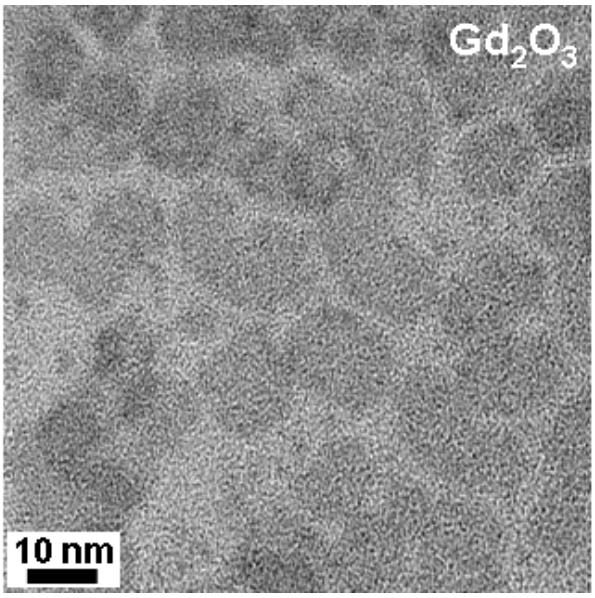

Figure S10. TEM image of the nanoparticle species obtained under stirred reflux conditions.

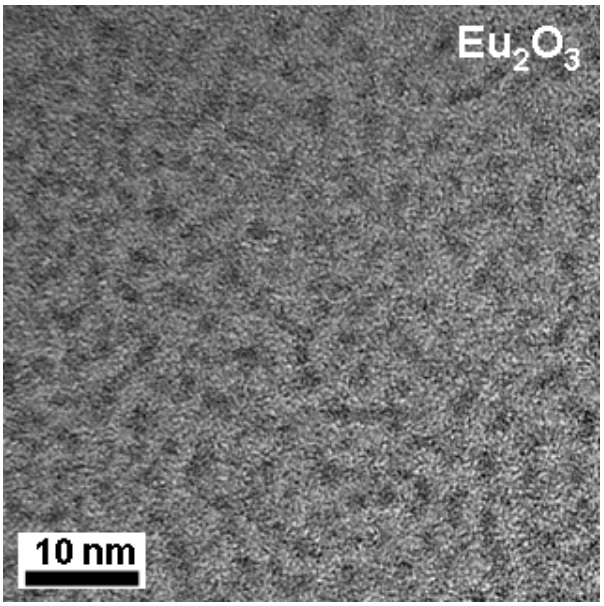

Figure S11. TEM image of the nanoparticle species obtained under unsealed autoclave conditions.

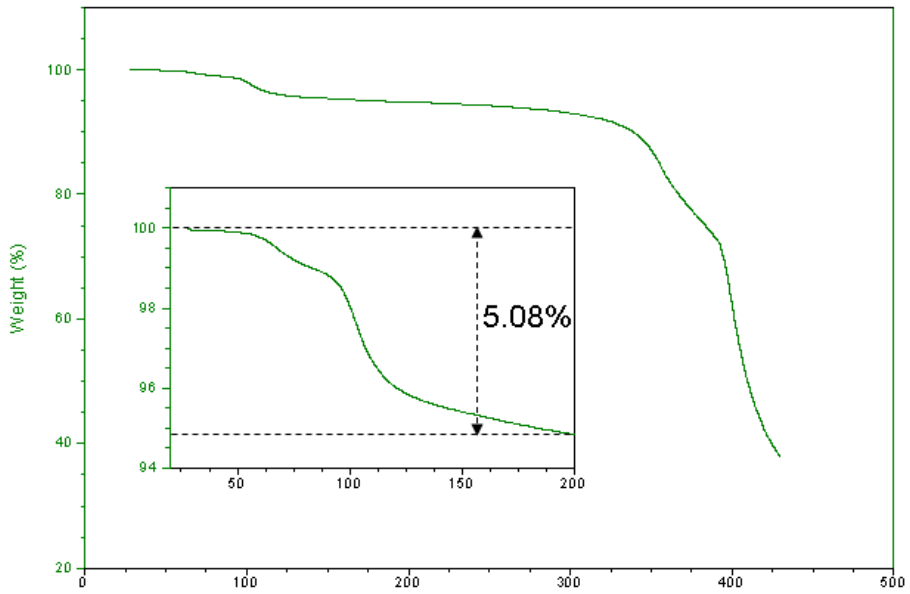

Figure S12. Thermogravimetric analysis curves showing the decomposition characteristics for a typical Europium oleate precursor. Inset is an expansion of the room temperature to 200 °C region, showing a weight loss of 5.08% attributable to the loss of crystal water.

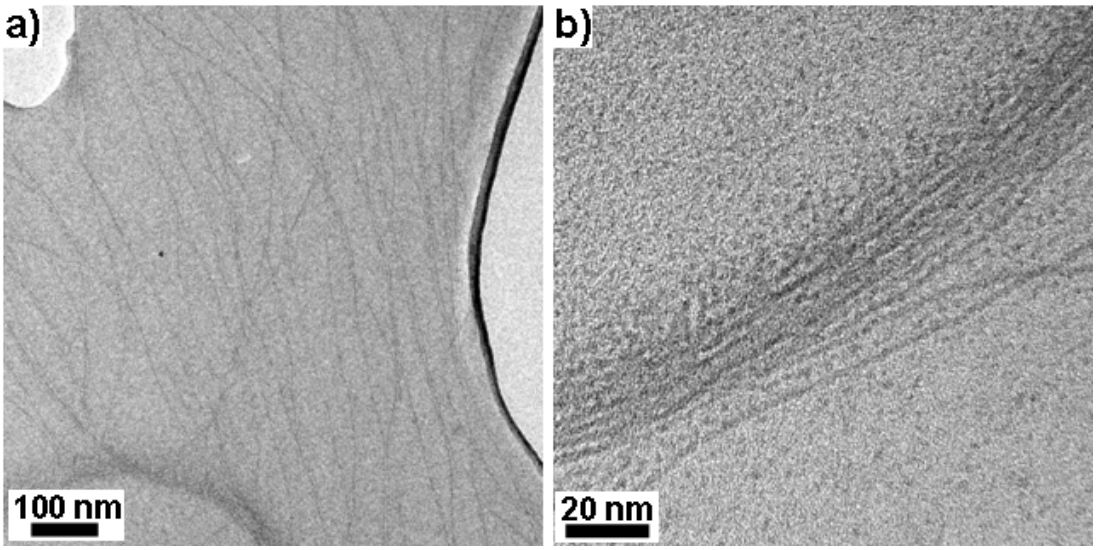

Figure S13. Low magnification (a) and high magnification (b) TEM images of Gd_2O_3 nanowires from a reaction performed with 2 mL additional water added.

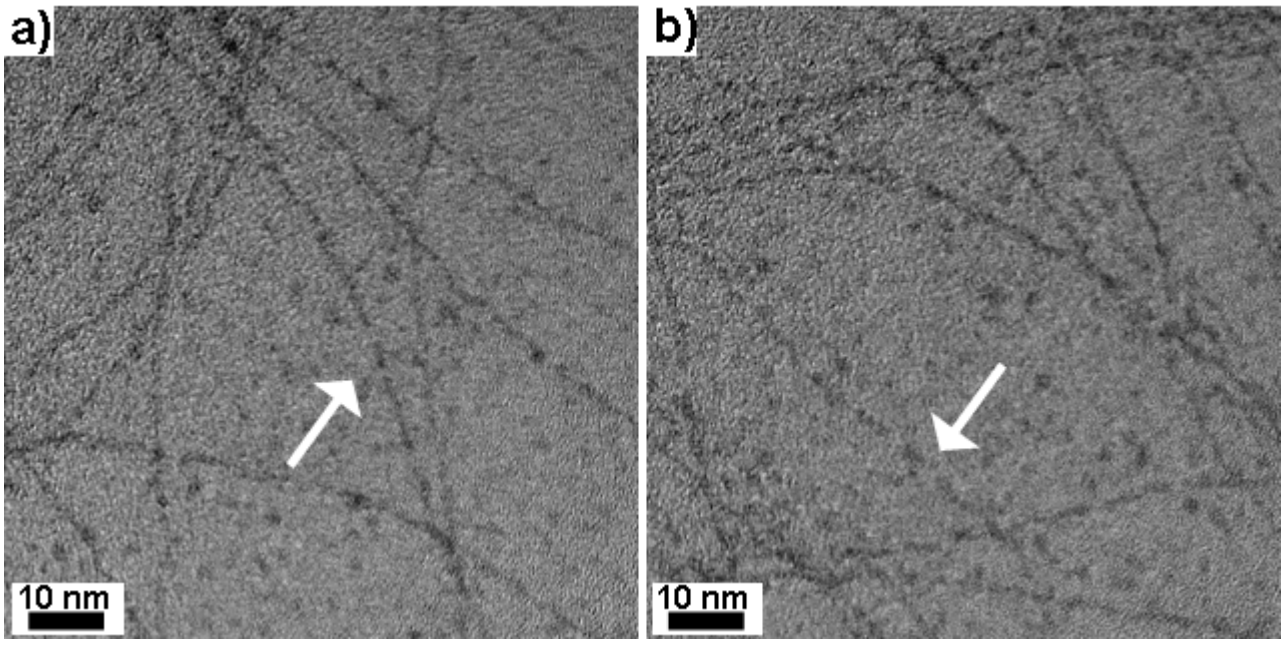

Figure S14. Additional TEM pictures of Gd_2O_3 wires obtained when benzyl ether was used instead of dioctyl ether. The white arrows indicate broken and crooked regions in the wires, indicative of a poorly defined reaction environment in which coalescence between adjacent particles is inadequate.

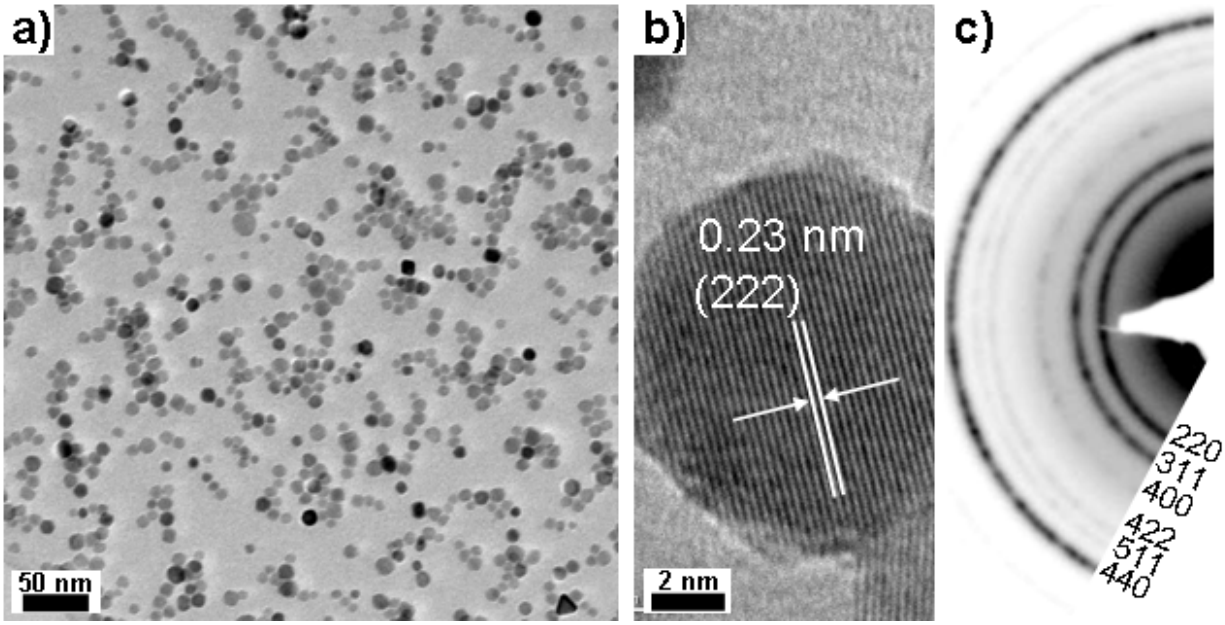

Figure S15. (a) TEM images of Fe_2O_3 nanoparticles obtained from the autoclave decomposition of Fe oleate under otherwise identical conditions to those used for Ln_2O_3 nanowire synthesis. (b) A HRTEM image of a single Fe_2O_3 NP, with (c) the corresponding ED pattern for a sample of the particles.

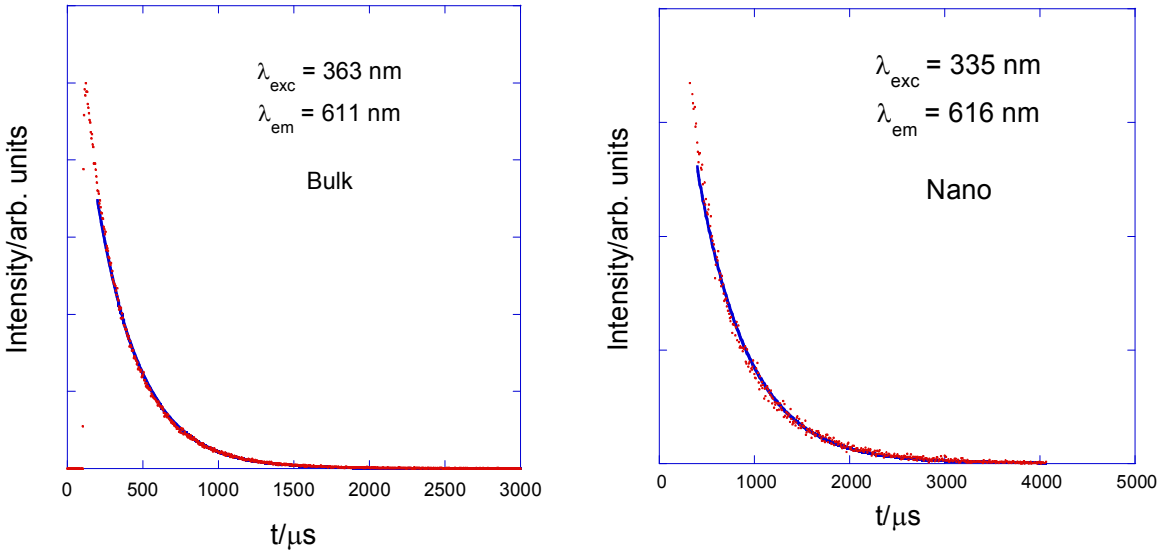

Figure S16. Temporal decay of the luminescence intensity for Eu_2O_3 in the bulk (left) and nanowires (right). The solid lines correspond to the least squares fittings to the experimental data to the equation: $I(t) = I_0 \exp(-t/\tau)$ with τ = 290 μs and 533 μs for bulk and nanowires, respectively.

Determining water content of the oleate precursor:

TGA analysis (Figs. S8 and S11) was used to measure the percentage weight change due to loss of water from the precursor. Figure S11 shows a 5.08% weight loss below 200 °C, which is in good agreement with the predicted percentage change assuming the loss of 3 waters from the $Eu(oleate)_3$ complex.

Determining contribution of water to reaction vessel pressure:

As the autoclave reaction temperature of 200 °C is above the boiling point of water, there will be a contribution to the pressure within the autoclave from the 0.5 mmol of lanthanide oleate present, which will contain 1.5 mmol of water.

Wu et al propose that water may also be generated in-situ by the condensation reaction between oleic acid and oleylamine.[5] In our system, a similar reaction could result in the formation of up to 9.5 mmol of water.

From this, a minimum and maximum reaction pressure can be calculated using two water contributions: the crystal water contribution and the crystal and condensation water contribution.

Using the van der Waals gas equation: $\mathbf{P= nRT/(V-nb) – n^2V/a^2}$

And assuming:
n = 0.0015 moles for the crystal water only contribution, or **n = 0.011** moles for the combined crystal and condensation water contributions
V = 0.003 L (derived from 12 mL autoclave volume minus 9 mL solvent volume, assuming solvent is non-compressible)
$\mathbf{R = 0.08206\ L\,atm\,K^{-1}\,mol^{-1}}$
T = 473 K
$\mathbf{a = 5.537\ L^2\ bar\ mol^{-2}}$
$\mathbf{b = 0.03049\ L\ mol^{-1}}$

we obtain minimum and maximum reaction pressure values of **18.32 atm** and **85.79 atm.**
As a control reaction performed in an unsealed autoclave failed to produce nanowires, we can conclude that wire formation requires elevated pressures. These pressures are generated in-situ as a result of steam formation from either the crystal water present in the oleate precursor, condensation between the acid and amine surfactants or a combination of both.

REFERENCES

[1] E. Hemmer, Y. Kohl, V. Colquhoun, H. Thielecke, K. Soga and S. Mathur, *J. Phys. Chem. B,* 2010, **114**, 4358.

[2] Z. Xu, C. Shen, Y. Hou, H. Gao and S. Sun, *Chem. Mater.,* 2009, **21**, 1778.

[3] K. Nakamoto, *Infrared and Raman Spectra of Inorganic and Coordination Compounds*, John Wiley & Sons, Ltd, 5th edn, 1997, p. 59.

[4] F. Söderlind, H. Pedersen, R. M. Petoral Jr., P.-O. Käll and K. Uvdal, *J. Colloid Interface Sci.*, 2005, **288**, 140.

[5] H. Wu, Y. Yang and Y. C. Cao, *J. Am. Chem. Soc.,* 2006, **128**, 16522.

[6] (a) J. A. Fortner, E. C. Buck, A. J. Ellison AND J. K. Bates, *Ultramicroscopy,* 1997, **67**, 77; (b) F. Xu and Y. Bando, *J. Appl. Phys.,* 2001, **89**, 5469.

[7] (a) L. Wu, H. Wiesmann, A. Moodenbaugh, R. Klie, Y. Zhu, D. Welch and M. Suenaga, *Phys. Rev. B,* 2004, **69**, 125415 (b) S. Tsunekawa, R. Sivamohan, S. Ito, A. Kasuya and T. Fukuda, *Nanostructured Materials,* 1999, **11**, 141.

[8] J. Conesa, *Surf. Sci.,* 1995, **339**, 337.